Molecular characterization of water-soluble aerosol particle-extracts by ultra-high resolution mass spectrometry: Observation of industrial emissions and an atmospherically aged wildfire plume at Lake Baikal

*Eric Schneider[1,2], Hendryk Czech[*1,3], Olga Popovicheva[4], Hannes Lüdtke[1,2], Jürgen Schnelle-Kreis[3], Tamara Khodzher[5], Christopher P. Rüger[*1,2], Ralf Zimmermann[1,2,3]*

1 – Joint Mass Spectrometry Centre (JMSC), Chair of Analytical Chemistry, University of Rostock, 18059 Rostock, Germany

2 – Department Life, Light & Matter (LLM), University of Rostock, 18059 Rostock, Germany

3 – Joint Mass Spectrometry Centre (JMSC) Cooperation Group "Comprehensive Molecular Analytics" (CMA) Helmholtz Zentrum München, 81379 Munich, Germany

4 – Skobeltsyn Institute of Nuclear Physics, Lomonosov Moscow State University, Leninskie Gory, 1, 119991 Moscow, Russia

5 – Limnological Institute, Siberian Branch of the Russian Academy of Sciences, 664033 Irkutsk, Russia

* – corresponding author: hendryk.czech@uni-rostock.de, christopher.rueger@uni-rostock.de

Table S1: List of samples collected in Lake Baikal expedition of 2018, with collection date, sampling time and volume, associated pollution sources as well as eBC and AAE data.[1]

Nr.	Route	Wind direction	Date	Start time	End time	Sampling time [h]	Volume [m³]	Pollution Sources	eBC [µg/m³]	AAE (Filter)
3	Tankhoi-Kultuk	NW	16.-17.07.2018	16.07.2018 20:00	17.07.2018 03:07	7	4.27	Coal burning, wildfires	2.1	3.6
4	Kultuk-Baikalsk	NW	17.07.2018	17.07.2018 03:07	17.07.2018 06:45	3.5	2.15	industrial FF, coal burning, BB	1.6	
5	Baikalsk	NW	17.07.2018	17.07.2018 06:57	17.07.2018 12:17	5	3.2	industrial FF, coal burning, BB	2.0	
6	Baikalsk-Boyarsk	NW	17.07.2018	17.07.2018 12:25	17.07.2018 21:31	9	5.46	Industrial FF		0.9
7	Boyarsk	NW	17.-18.07.2018	17.07.2018 21:35	18.07.2018 07:25	10	5.9	Coal burning, wildfires	1.7	3.6
8	Boyarsk	NW	18.07.2018	18.07.2018 07:30	18.07.2018 16:50	9.5	5.6	Industrial FF	1.4	
9	Boyarsk-Selenga	NE	18.-19.07.2018	18.07.2018 17:00	19.07.2018 00:25	7.5	4.45	Coal burning, wildfires	1.4	3
10	Selenga-Listvyanka	NE	19.07.2018	19.07.2018 00:25	19.07.2018 08:15	7.75	4.65	~	1.7	
11	Bolshie Koty-Olchonskie Vorota	E	20.07.2018	19.07.2018 12:40	20.07.2018 01:10	12	7.5	Residential BB		1.8
12	OlchonskieVorota-Ogoy	E	20.07.2018	20.07.2018 01:25	20.07.2018 07:25	6	3.4	Residential coal burning, BB	0.8	3.5
13	Ogoy - Khuzhir	E	20.07.2018	20.07.2018 09:10	20.07.2018 17:05	8	4.75	Residential coal burning, BB	1.1	2.2
14	Khuzhir - Nizhneangarsk	E	21.07.2018	20.07.2018 17:10	21.07.2018 22:45	6	15.05	Local BC	0.8	1.1
15	Nizhneangarsk-Severobaikalsk	N	22.07.2018	21.07.2018 22:45	22.07.2018 11:50	12.75	8.15	Wildfires	1.3	1.5
16	Severobaykalsk-Khakusy	N	22.07.2018	22.07.2018 12:15	22.07.2018 19:00	6.75	4.05	Wildfires		2
17	Khakusy-Uskaniy Island	N	23.07.2018	22.07.2018 19:00	23.07.2018 08:55	14	8.35	Wildfires		1.8
18	Ushkany Island- Barguzinsky bay	N	23.07.2018	23.07.2018 12:15	23.07.2018 18:15	6	3.6	Wildfires	1.9	1.7
19	Ust-Barguzinsky	N	24.07.2018	23.07.2018 18:10	24.07.2018 06:00	12	7	Wildfires	2.5	1.5
20	Barguzinsky bay – Selenga river	N	25.07.2018	24.07.2018 06:15	25.07.2018 03:15	21	9.45	Industrial FF	1.9	0.9
21	Selenga river	SW	25.07.2018	25.07.2018 03:20	25.07.2018 12:10	9	5.3	Residential BB	1.8	2.2
22	Selenga- Peschanka-Bolshie Koty	NW	26.07.2018	25.07.2018 12:10	26.07.2018 09:07	21	9.55	Shipping, residential BB, wildfires	3.4	2.2

Table S2: Compound classes and the respective values used for calculation of saturation vapour pressure ($\log(C^*)$) obtained by least-squares optimization using the NCI database.[2]

Compound class	n_C^0	b_c	b_O	b_{CO}	b_n	b_s
CH	23.8	0.4861				
CHO	22.66	0.4481	1.656	−0.7790		
CHN	24.59	0.4066			0.9619	
CHON	24.13	0.3667	0.7732	−0.07790	1.114	
CHOS	24.06	0.3637	1.327	−0.3988		0.7579
CHONS	28.5	0.3848	1.011	0.2921	1.053	1.316

Table S3. Summed intensities of compound class groups and relative intensity of sum formula groups in positive and negative ionization mode.

Nr.	Intensity [a.u.], normalised to Sampling Volume				relative intensity [%]					
	CHO	CHN1O	CHN2O	CHOS1	aliphatic	high uns. & low oxy.	high uns. & high oxy.	polyphenols	condensed aromatics	
3	2.50E+09	2.14E+09	4.37E+08	8.30E+08	0.2742	0.0310	0.0013	0.0635	0.0248	positive
4	4.28E+09	3.42E+09	1.00E+09	8.03E+08	0.2396	0.0003	0.0	0.0191	0.0020	
5	3.38E+09	2.01E+09	8.46E+08	1.23E+08	0.2334	0.0047	0.0	0.0190	0.0017	
6	1.94E+09	4.41E+08	5.82E+07	2.66E+07	0.4571	0.0434	0.0009	0.0365	0.0091	
7	3.11E+09	2.65E+09	1.17E+09	7.68E+08	0.4380	0.0297	0.0	0.0400	0.0040	
8	2.28E+09	1.46E+09	3.17E+08	5.40E+08	0.2261	0.0137	0.0	0.0319	0.0057	
9	2.76E+09	1.50E+09	1.98E+08	4.57E+08	0.2711	0.0375	0.0044	0.0509	0.0171	
10	2.23E+09	1.21E+09	1.98E+08	5.76E+08	0.2063	0.0114	0.0	0.0326	0.0054	
11	1.15E+09	5.64E+08	1.74E+08	4.22E+08	0.1504	0.0107	0.0003	0.0398	0.0170	
12	3.41E+09	3.19E+09	4.00E+08	5.60E+08	0.2605	0.0122	0.0007	0.0355	0.0140	
13	2.08E+09	1.14E+09	4.15E+08	4.09E+08	0.1849	0.0059	0.0	0.0238	0.0040	
14	6.21E+08	3.82E+08	2.26E+08	2.01E+08	0.1953	0.0054	0.0	0.0218	0.0033	
15	7.12E+08	6.41E+08	2.34E+08	1.84E+08	0.1367	0.0007	0.0001	0.0225	0.0060	
16	1.47E+09	2.17E+09	2.09E+08	3.59E+08	0.2546	0.0024	0.0011	0.0544	0.0194	
17	9.33E+08	6.59E+08	1.33E+08	3.05E+08	0.1924	0.0067	0.0001	0.0310	0.0065	
18	3.77E+09	2.30E+09	5.34E+08	9.24E+08	0.2336	0.0106	0.0002	0.0387	0.0072	
19	1.57E+09	1.08E+09	2.98E+08	4.34E+08	0.2285	0.0087	0.0	0.0300	0.0045	
20	1.36E+09	8.31E+08	1.71E+08	3.33E+08	0.2597	0.0195	0.0001	0.0349	0.0081	
21	2.32E+09	6.61E+08	9.63E+07	9.81E+07	0.4089	0.0314	0.0	0.0276	0.0064	
22	1.55E+09	8.72E+08	2.19E+08	1.74E+08	0.3941	0.0458	0.0038	0.0642	0.0124	
3	1.77E+09	4.81E+08	2.75E+08	1.99E+08	0.1249	0.2028	0.0020	0.0581	0.0539	negative
4	1.37E+09	7.38E+08	3.07E+08	7.21E+08	0.0527	0.0406	0.0010	0.0497	0.0168	
5	2.03E+09	6.03E+08	3.74E+08	2.66E+08	0.1293	0.1892	0.0030	0.0507	0.0312	
6	9.01E+08	2.89E+08	6.63E+07	1.76E+08	0.0712	0.2083	0.0049	0.0883	0.0985	
7	1.26E+09	1.90E+08	6.77E+08	2.39E+08	0.1329	0.3889	0.0148	0.0699	0.3537	
8	1.20E+09	3.11E+08	1.33E+08	2.90E+08	0.1498	0.2758	0.0091	0.0543	0.0443	
9	9.23E+08	2.10E+08	1.15E+08	8.00E+08	0.6340	0.1745	0.0076	0.0808	0.0914	
10	1.82E+09	4.32E+08	3.09E+08	2.00E+08	0.1589	0.2395	0.0021	0.0450	0.0347	
11	1.09E+09	2.08E+08	1.94E+08	2.04E+08	0.1403	0.2406	0.0022	0.0496	0.0408	
12	1.76E+09	4.30E+08	3.22E+08	3.22E+08	0.1237	0.2084	0.0016	0.0899	0.0660	
13	1.06E+09	2.45E+08	2.65E+08	1.24E+08	0.1545	0.1522	0.0011	0.0522	0.0319	
14	4.59E+08	1.18E+08	1.13E+08	5.37E+07	0.2078	0.1897	0.0008	0.0450	0.0333	
15	4.90E+08	2.09E+08	6.59E+07	7.76E+07	0.1297	0.1441	0.0032	0.0747	0.0384	
16	1.31E+08	1.34E+08	6.48E+07	1.16E+08	0.1320	0.0304	0.0063	0.0793	0.0354	
17	5.99E+08	2.00E+08	8.46E+07	7.08E+07	0.0996	0.2333	0.0049	0.0563	0.0398	
18	1.43E+09	4.56E+08	2.20E+08	1.36E+08	0.1091	0.2223	0.0029	0.0526	0.0315	
19	9.30E+08	2.38E+08	1.13E+08	4.27E+07	0.1256	0.2946	0.0109	0.0660	0.0262	
20	8.95E+08	2.06E+08	1.02E+08	6.58E+07	0.1517	0.3905	0.0090	0.0610	0.0393	
21	8.24E+08	2.54E+08	6.88E+07	1.22E+08	0.0493	0.2022	0.0038	0.0601	0.0650	
22	7.66E+08	1.99E+08	5.96E+07	1.30E+08	0.1136	0.4023	0.0093	0.0787	0.0935	

Table S4: Relative number of sum formula with O/N ratio below or higher three and five in ESI(+/-) with calculated average and standard deviation.

	Number Percentage					
Nr.	positive O/N<3	positive O/N>=3	positive O/N>=5	negative O/N<3	negative O/N>=3	negative O/N>=5
3	21.7	52.8	25.5	11.8	60.7	27.6
4	36.4	49.7	13.9	12.7	58.9	28.3
5	30.9	51.7	17.4	9.6	63.8	26.6
6	22.1	56.4	21.6	14.1	55.2	30.7
7	22.1	57.2	20.7	10.0	64.7	25.3
8	28.9	50.7	20.4	12.6	60.2	27.1
9	25.5	51.5	23.0	15.0	69.4	15.6
10	30.1	50.1	19.8	7.9	62.9	29.1
11	37.0	46.3	16.6	12.8	61.1	26.1
12	22.8	53.6	23.5	9.7	60.3	30.0
13	33.2	50.6	16.2	13.1	58.9	28.0
14	32.0	50.5	17.5	11.4	60.0	28.6
15	34.2	50.3	15.5	9.1	61.0	29.9
16	19.4	56.4	24.2	18.9	57.5	23.6
17	27.6	50.8	21.5	9.4	64.8	25.8
18	31.4	49.2	19.4	4.3	64.1	31.6
19	29.8	50.0	20.3	9.0	63.7	27.3
20	24.9	52.4	22.7	6.8	64.7	28.5
21	24.7	55.0	20.3	7.1	61.7	31.2
22	23.4	54.5	22.2	8.6	64.8	26.6
av	27.91	51.99	20.10	10.71	61.92	27.37
std	5.1	2.7	3.0	3.2	3.1	3.4

Table S5: Relative number of sum formula with O/S ratio below or higher four and seven in ESI (+/-) with calculated average and standard deviation.

	Number Percentage [%]					
Nr.	**positive O/S<4**	**positive O/S>=4**	**positive O/S>=7**	**negative O/S<4**	**negative O/S>=4**	**negative O/S>=7**
3	14.27	37.05	48.69	70.17	13.54	16.28
4	35.84	45.74	18.42	73.46	6.70	19.84
5	50.81	32.26	16.94	64.24	17.66	18.10
6	45.28	32.08	22.64	87.18	4.68	8.15
7	19.56	28.00	52.44	31.00	18.09	50.91
8	22.31	48.53	29.16	47.30	21.40	31.30
9	20.08	34.40	45.52	51.33	21.67	27.00
10	22.40	51.55	26.05	57.35	15.59	27.06
11	30.41	45.29	24.30	49.30	19.61	31.09
12	17.18	26.93	55.88	81.94	8.86	9.20
13	28.06	47.22	24.72	66.38	16.81	16.81
14	27.34	47.52	25.14	64.39	15.86	19.75
15	47.27	41.59	11.14	73.29	13.25	13.47
16	14.26	19.01	66.73	69.03	18.58	12.39
17	30.15	50.60	19.25	58.24	18.51	23.25
18	24.48	33.26	42.26	68.75	12.50	18.75
19	19.20	53.93	26.88	54.68	22.66	22.66
20	15.12	49.91	34.97	50.08	22.57	27.36
21	40.37	36.70	22.94	80.87	10.43	8.70
22	26.85	31.29	41.86	60.97	13.19	25.85
av	27.56	39.64	32.80	63.00	15.61	21.40
std	10.9	9.6	14.6	13.2	5.0	9.7

Table S6. Intensity weighted average OM/OC ratio of each sample in ESI+/-.

Nr.	OM/OC	
	ESI+	ESI-
3	2.80	2.81
4	2.98	2.64
5	2.95	2.83
6	2.91	2.62
7	2.83	2.69
8	2.88	2.90
9	2.87	3.09
10	2.89	2.90
11	2.80	2.91
12	2.87	2.76
13	2.95	2.87
14	2.89	2.91
15	2.91	2.69
16	2.84	2.62
17	2.87	2.81
18	2.86	2.83
19	2.85	2.84
20	2.85	2.88
21	2.92	2.69
22	2.80	2.80

Table S7: Relative intensity of assigned organic aerosol classes in negative and positive ionization mode separated into by CHO, CHON and CHOS compound class.

		CHO [%]					CHON [%]					CHOS [%]				
	Nr.	**LVOOA**	**BBOA**	**SVOOA**	**HOA**	**Oligomers**	**LVOOA**	**BBOA**	**SVOOA**	**HOA**	**Oligomers**	**LVOOA**	**BBOA**	**SVOOA**	**HOA**	**Oligomers**
negative ESI	3	19.8	0.0	4.7	0.0	28.8	23.5	0.2	5.5	0.0	51.0	4.0	1.5	2.8	0.0	29.8
	4	8.2	1.3	1.1	1.3	27.7	9.7	1.4	2.0	1.3	55.3	1.8	3.6	2.7	0.4	47.2
	5	20.8	0.2	3.3	0.2	27.6	24.6	0.5	4.0	0.2	51.7	4.1	1.0	1.9	0.0	32.3
	6	25.6	0.0	6.9	0.0	22.1	30.4	0.1	7.9	0.0	36.6	5.5	1.5	4.8	0.0	22.8
	7	27.8	0.0	2.8	0.0	16.0	31.9	0.0	3.3	0.0	48.4	6.3	0.5	1.1	0.0	40.4
	8	26.3	0.3	3.0	0.3	21.4	31.4	0.3	3.9	0.3	36.5	8.5	0.7	1.9	0.0	30.4
	9	5.4	0.0	0.3	0.0	5.4	10.5	0.1	0.8	0.0	10.1	5.8	30.0	10.4	0.1	23.9
	10	19.1	0.0	4.0	0.0	32.9	22.3	0.1	4.4	0.0	56.6	4.5	1.2	1.5	0.0	29.7
	11	18.5	0.0	2.9	0.0	30.7	22.3	0.1	3.3	0.0	52.7	5.3	0.8	2.5	0.0	33.0
	12	15.1	0.0	5.0	0.0	33.8	17.9	0.1	5.4	0.0	54.0	3.4	2.1	3.7	0.0	28.9
	13	11.8	0.1	3.0	0.1	36.5	13.9	0.7	3.6	0.1	64.6	2.3	1.7	2.5	0.0	35.3
	14	11.8	0.1	3.9	0.0	34.7	13.9	0.2	4.4	0.0	62.5	2.9	0.6	1.7	0.0	37.1
	15	16.3	0.1	1.6	0.0	29.2	19.7	0.2	2.4	0.0	55.4	3.5	3.6	3.0	0.0	33.4
	16	6.4	0.3	4.2	0.0	11.2	11.2	1.7	5.6	0.0	43.3	6.4	3.8	2.2	0.0	51.5
	17	22.4	0.0	2.5	0.0	27.7	16.0	0.2	3.2	0.0	26.4	5.2	0.9	2.0	0.0	31.7
	18	21.6	0.1	3.8	0.0	31.6	3.8	0.3	0.8	0.1	21.4	4.4	0.7	2.0	0.1	26.6
	19	30.6	0.0	3.1	0.0	25.0	5.1	0.2	0.9	0.0	20.7	5.5	0.3	1.1	0.1	27.6
	20	34.0	0.0	3.7	0.0	21.6	5.7	0.1	0.6	0.0	17.9	6.3	0.7	1.4	0.0	25.4
	21	28.6	0.2	4.4	0.1	23.7	5.1	0.2	0.5	0.0	15.3	5.4	1.1	4.0	0.0	21.7
	22	33.5	0.0	4.2	0.0	18.3	6.4	0.1	0.4	0.0	14.6	9.1	0.8	3.7	0.0	22.1
positive ESI	3	0.3	2.5	2.3	0.1	32.9	1.6	2.4	1.3	0.6	40.2	1.6	2.6	1.6	0.6	52.7
	4	0.0	4.1	2.6	0.9	29.5	0.0	5.3	1.0	7.0	35.2	0.1	5.5	1.2	7.0	42.0
	5	0.0	2.5	1.7	0.2	40.6	0.0	4.2	1.1	2.2	39.6	0.0	4.2	1.2	2.2	41.2
	6	0.2	9.4	7.7	0.9	55.9	0.4	2.6	1.3	1.1	15.5	0.5	2.6	1.3	1.1	16.5
	7	0.0	1.5	1.5	0.1	35.0	0.0	1.8	1.0	0.2	47.2	0.0	1.9	1.2	0.2	56.3
	8	0.0	2.2	2.2	0.1	38.8	0.0	4.0	2.0	1.5	35.9	0.0	4.2	2.1	1.5	46.0
	9	0.3	4.6	4.5	0.3	39.9	3.1	3.3	1.7	2.2	26.2	3.8	3.3	1.8	2.3	33.3
	10	0.0	2.3	1.9	0.2	38.3	0.0	4.3	1.5	2.5	31.3	0.0	4.3	1.6	2.6	42.5
	11	0.1	2.8	2.4	0.1	37.1	0.5	4.0	2.1	2.4	28.5	0.6	4.4	3.1	2.4	43.6
	12	0.2	4.3	2.9	0.6	32.2	1.1	3.4	1.2	3.4	39.0	1.1	3.6	1.3	3.5	45.2
	13	0.0	2.9	2.1	0.4	37.3	0.0	4.6	1.5	3.9	33.7	0.0	4.9	1.7	3.9	42.0
	14	0.0	1.7	1.6	0.2	31.7	0.0	3.5	1.3	1.5	40.5	0.0	3.7	1.6	1.5	51.7
	15	0.0	3.7	2.5	0.5	26.9	0.2	5.8	1.1	6.0	38.4	0.2	6.0	1.6	6.0	47.1
	16	0.4	5.4	2.8	0.7	21.0	1.6	3.1	0.8	4.0	43.8	1.7	3.1	0.9	4.0	51.3
	17	0.0	3.1	2.5	0.2	33.8	0.2	4.1	1.6	1.9	35.6	0.2	4.4	2.0	2.0	48.0
	18	0.1	2.3	2.2	0.3	36.0	0.2	3.6	1.3	1.9	34.5	0.2	3.7	1.5	1.9	44.5
	19	0.0	1.9	1.6	0.1	36.7	0.0	3.4	1.4	1.4	38.3	0.0	3.5	1.5	1.4	49.4
	20	0.0	2.3	2.3	0.1	40.1	0.1	2.6	1.4	0.8	35.7	0.1	2.7	1.6	0.8	46.5
	21	0.1	8.9	6.1	1.1	51.5	0.1	2.9	1.2	2.3	18.1	0.1	2.9	1.2	2.4	20.8
	22	0.1	4.3	3.9	0.3	43.1	1.9	2.4	1.4	0.7	33.8	2.1	2.6	1.8	0.7	38.9

Table S8. Intensity weighted average parameter of each filter extract in positive and negative ionisation mode.

Nr.	positive							negative						
	H/C	O/C	N/C	S/C	DBE	OS_C	AI_{mod}	H/C	O/C	N/C	S/C	DBE	OS_C	AI_{mod}
3	1.43	0.33	0.030	0.005	8.53	-0.78	0.24	1.28	0.49	0.034	0.010	8.32	-0.31	0.28
4	1.72	0.22	0.036	0.005	4.96	-1.28	0.16	1.28	0.33	0.027	0.013	9.95	-0.62	0.29
5	1.62	0.29	0.036	0.003	6.03	-1.05	0.16	1.30	0.48	0.036	0.010	8.08	-0.33	0.28
6	1.55	0.34	0.017	0.001	5.33	-0.86	0.19	1.13	0.45	0.024	0.012	9.32	-0.23	0.35
7	1.47	0.32	0.033	0.004	8.17	-0.83	0.21	1.12	0.51	0.049	0.012	8.76	-0.10	0.28
8	1.53	0.31	0.035	0.004	7.06	-0.90	0.19	1.29	0.55	0.030	0.021	7.41	-0.20	0.29
9	1.49	0.35	0.029	0.005	6.61	-0.79	0.23	1.43	0.51	0.068	0.084	6.17	-0.41	0.39
10	1.56	0.29	0.032	0.006	6.92	-0.99	0.19	1.34	0.52	0.034	0.009	7.66	-0.30	0.26
11	1.48	0.28	0.032	0.007	8.09	-0.92	0.22	1.33	0.53	0.038	0.013	7.84	-0.28	0.25
12	1.53	0.30	0.032	0.004	6.81	-0.94	0.22	1.26	0.46	0.028	0.011	8.79	-0.35	0.29
13	1.63	0.28	0.038	0.004	6.18	-1.07	0.16	1.36	0.47	0.041	0.009	8.01	-0.43	0.25
14	1.57	0.28	0.040	0.006	7.04	-1.01	0.18	1.39	0.47	0.037	0.011	7.60	-0.44	0.24
15	1.63	0.23	0.044	0.004	6.00	-1.17	0.19	1.23	0.41	0.031	0.011	9.24	-0.41	0.31
16	1.52	0.28	0.035	0.006	6.68	-0.95	0.24	1.24	0.32	0.041	0.021	9.25	-0.60	0.37
17	1.55	0.29	0.035	0.005	6.98	-0.97	0.20	1.27	0.51	0.036	0.008	8.37	-0.26	0.28
18	1.54	0.28	0.032	0.005	7.24	-0.98	0.20	1.29	0.50	0.030	0.008	7.93	-0.28	0.26
19	1.52	0.29	0.035	0.005	7.48	-0.95	0.19	1.26	0.54	0.032	0.008	7.91	-0.18	0.27
20	1.50	0.31	0.030	0.005	7.46	-0.87	0.20	1.27	0.57	0.031	0.009	7.53	-0.14	0.27
21	1.59	0.31	0.020	0.002	5.21	-0.96	0.18	1.16	0.49	0.026	0.010	8.99	-0.19	0.34
22	1.44	0.33	0.028	0.003	7.43	-0.77	0.24	1.20	0.55	0.028	0.015	8.00	-0.10	0.32

Detailed description of ESI+/- FTICR-MS mass spectra

In both cases of Figure 3, the molecular complexity of the three compound classes in the range of *m/z* 150 to 650 for the industrial and *m/z* 150 to 700 for the *WF-Yakutia* sample is high. The exemplary wildfire-affected sample *WF-Yakutia* (right) shows a higher relative abundance of CHOS compounds, present in the mass range between *m/z* 250 and 600. The whole mass range is shared by a distribution of CHON compounds from m/z 200 to 700, whose relative abundance is higher in the *WF-Yakutia* sample than in the *industrial* sample. The CHO class is abundant over the whole mass range in both cases, with higher intensities in the lower mass range for the *industrial* sample, compared to the more even intensity distribution over the whole mass range for *WF-Yakutia*. The described sum formula distributions are in good agreement with the observed relative abundance of oxygen atoms in each compound class (Figure S3). The CHO class of the exemplary *WF-Yakutia* sample displays a bimodal distribution of oxygen atoms with maxima at 4 and 15. $CHON_1$ and $CHOS_1$ class both display a single distribution with a maximum at 8 oxygen atoms while the $CHON_2$ class has a maximum at 7 oxygen atoms and another protruding peak at 2 oxygen atoms. Sodium adducts are more abundant for highly oxygenated species with four or more oxygen atoms which are consequently more commonly found in the higher mass range (Figure S3). A consistent distribution of CHO compounds is also found in ESI-, with *WF-Yakutia* showing an exceptionally small number of signals (Figure S6). CHOS compounds, which may be more sensitively detected in negative ionization mode, display a similar behavior with a unimodal distribution for the industrial sample, centered around *m/z* 350. CHON compounds are detected in the mass range between *m/z* 200 and 500, high molecular weight species are less abundant than in ESI+. This can again be explained by the lower sensitivity for the less acidic nitrogen containing molecular groups in ESI- as well as the lower number of sum formulas detected in general. Nitrogen-containing WSOA are discussed to play an important role in the composition of BrC.[3] They are also a main part of the aged OA over Lake Baikal, suggesting that some species are emitted from biomass burning or generated through atmospheric aging reactions. Especially when comparing the wildfire samples of differently aged OA from Yakutia (Figure 3 right) and Krasnoyarsk regions (Figure S7 right), distinct differences in the CHON class abundance are visible, as well as in the distribution pattern of the CHO and CHOS classes. The *WF-Yakutia* sample (*Sample 16*) is influenced by 5-day old air masses carrying WF emissions, while the *WF-Krasnoyarsk* sample (*Sample 20*) is influenced by air masses not older than one day. This can explain the higher abundancy of nitrogen-containing compounds, generated by atmospheric aging reactions in the *WF-Yakutia* sample. The *background* sample over Lake Baikal (*Sample 10,* Figure S7 left), with no direct emission sources, shows a mix of compound classes, and many signals that are also found in *WF* and *industrial* samples. This highlights the influence of atmospheric aging and long-range transport of primary emissions.

Fingerprint plots of elemental ratios

Van Krevelen (VK) plots of O/C and H/C ratios are commonly used to visualize differences and similarities of complex high-resolution MS data.[4] Due to the high abundance of nitrogen and sulfur as heteroatoms it is possible to also discuss S/C and N/C ratio plots of respective molecules as another measure for structural grouping of complex datasets. Intensity weighted average values for each sample of discussed elemental ratios as well as AI_{mod} and OS_C are given in Table S8. As expected from ambient aerosol samples with influences from primary and secondary emission sources, the overall difference in mean elemental composition between background, industrial and wildfire emissions influenced WSOA is moderately low, but some areas in the VK space display variations (Figure 6 and S12). Distinct sequences of homologous series (e.g. $-CH_2-$, -O-, …) are also visible in both diagrams and could be explained by products of incomplete combustion of biopolymers like lignin or cellulose, which break down at different positions of the polymer-like molecular structure, and by atmospheric aging.[5] The OS_C, as indicated by the red dotted lines, show that for ESI+, most sum formulae are found within the defined OS_C range of SV-OOA and BBOA, if only O/C and H/C are considered. This could again be an indicator for oligomerization products, formed from monomer species that are assigned to these classes, as oligomerization reactions maintain the OS_C, O/C and H/C ratio, but increase the carbon number.

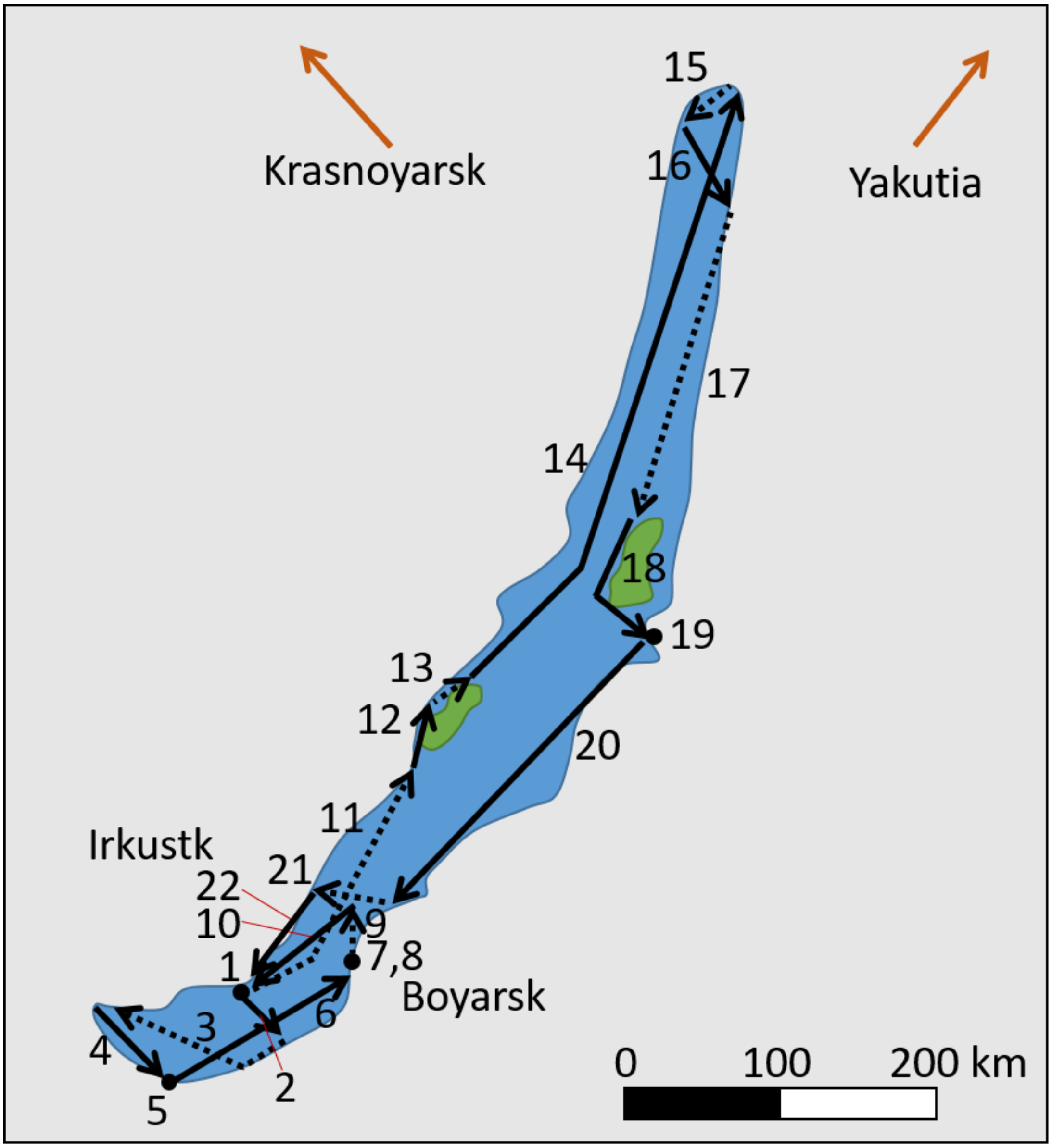

Figure S1: Schematic map of Lake Baikal with expedition route track and sampling points indicated by black lines (even sample number: solid-line, odd sample number: dashed line, stationary sampling: black dot).[1]

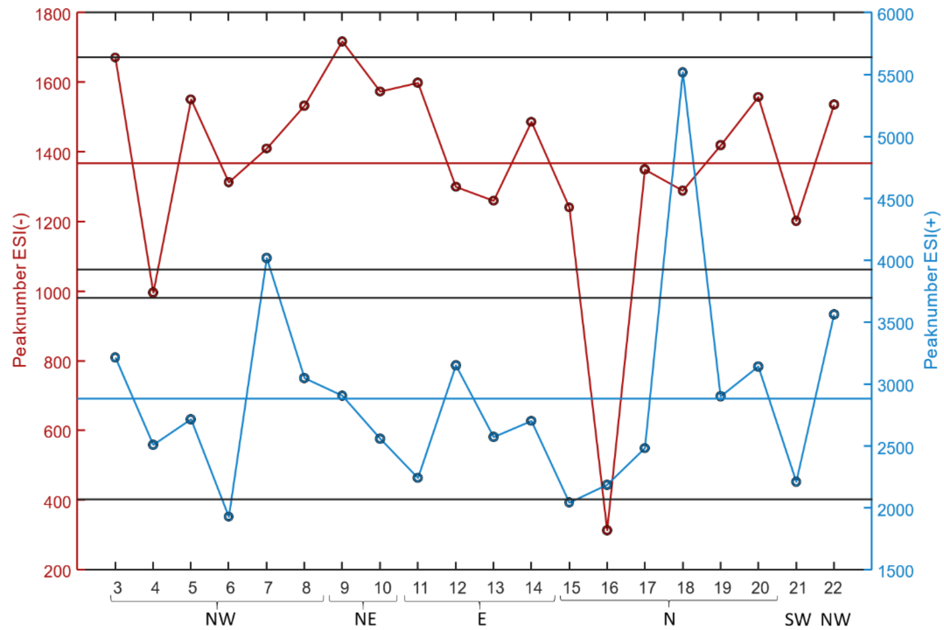

Figure S2. Absolute number of all sum formulae assigned from filter extract measurements in positive and negative ionization mode. Dotted line indicating respective mean values and solid lines representing distance of one standard deviation from mean value. Samples are assigned with the wind direction during their sampling.

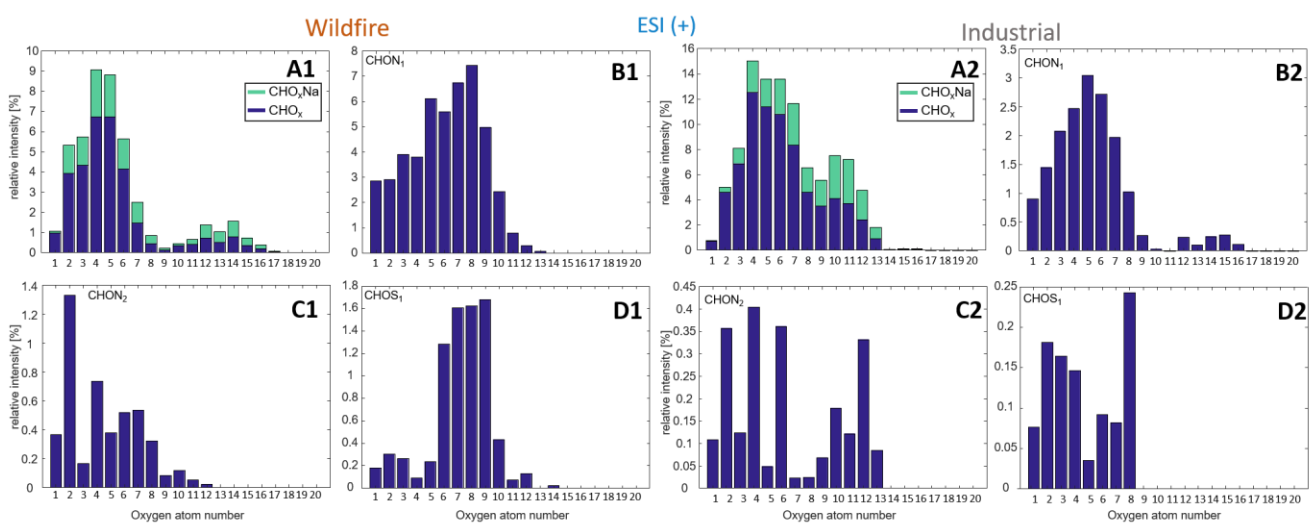

Figure S3. Relative abundance of oxygen atoms in each compound class with ESI+ of *WF-Yakutia (A1-D1, Sample 16)* and *industrial (A2-D2, Sample 6)*. **A**: Oxygen distribution with differentiation between Na^+ (green) and H^+ adducts (dark blue) of CHO class showing bimodal distribution with two maxima. **B**: Oxygen distribution of $CHON_1$ class. **C**: Oxygen distribution of $CHON_2$ class with. **D**: Oxygen distribution of CHOS class.

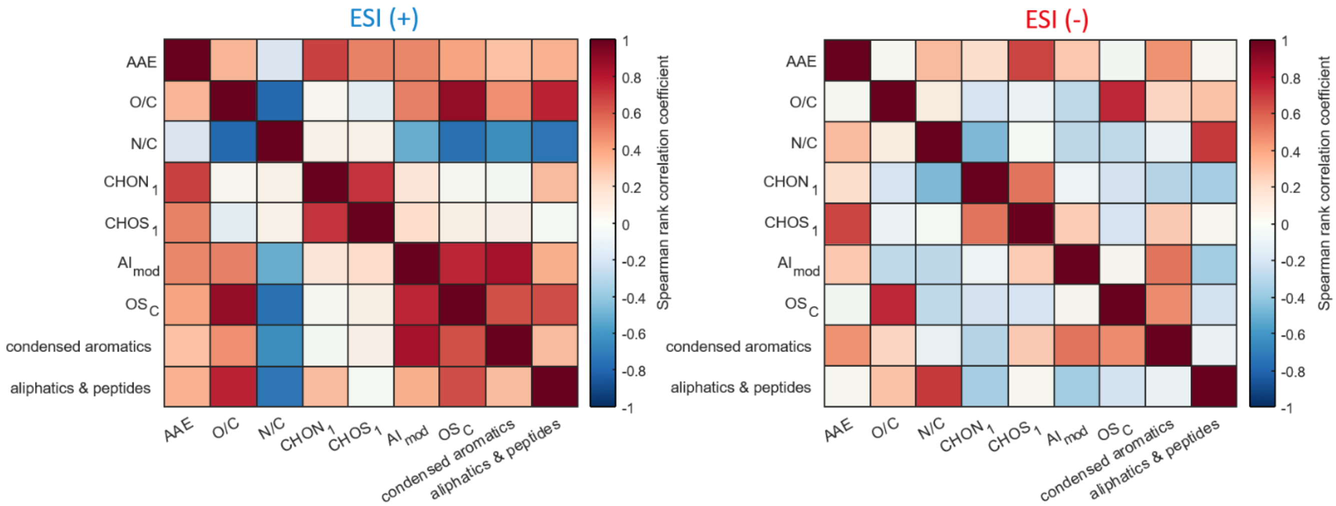

Figure S4. Spearman rank correlation coefficient matrix of chosen sum parameters in negative (right) and positive (left) ionization mode.

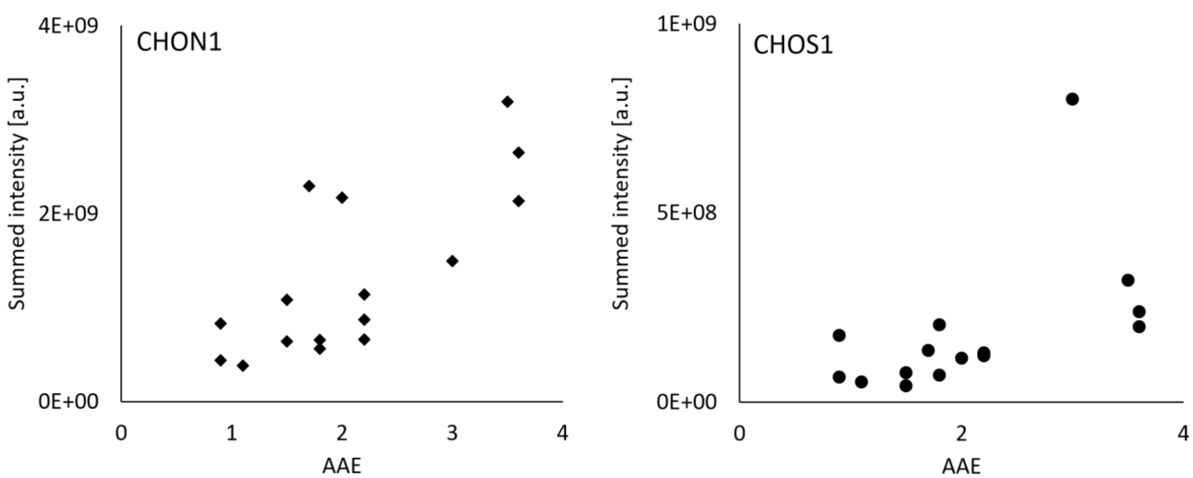

Figure S5: Correlation of $CHON_1$ (**A**, ESI+, r_S= 0.68, p<0.05) and $CHOS_1$ (**B**, ESI-, r_S= 0.62, p<0.05) compound classes summed intensity with AAE data.

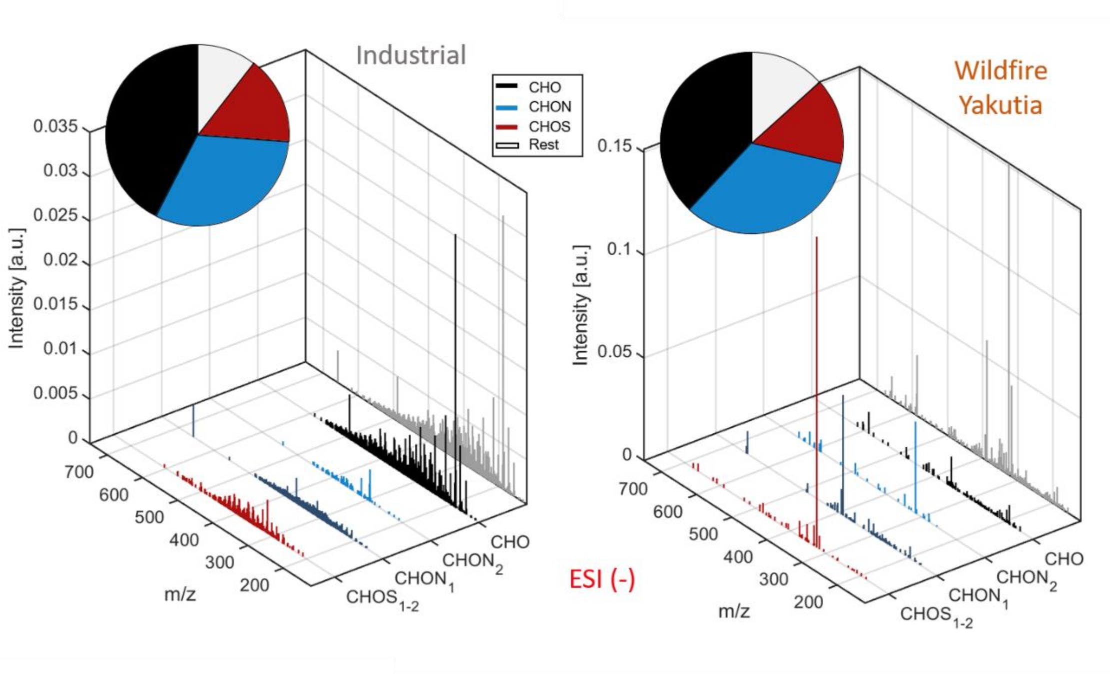

Figure S6. ESI (-)-FTICR mass spectra of exemplary industrial (left, *Sample 6*) and wildfire influenced (right, *Sample 16)* filter extract, normalized to TIC, as well as pie charts of the relative sum formula number of each compound class. Only CHO (black), CHON (blue) and CHOS (red) species are shown.

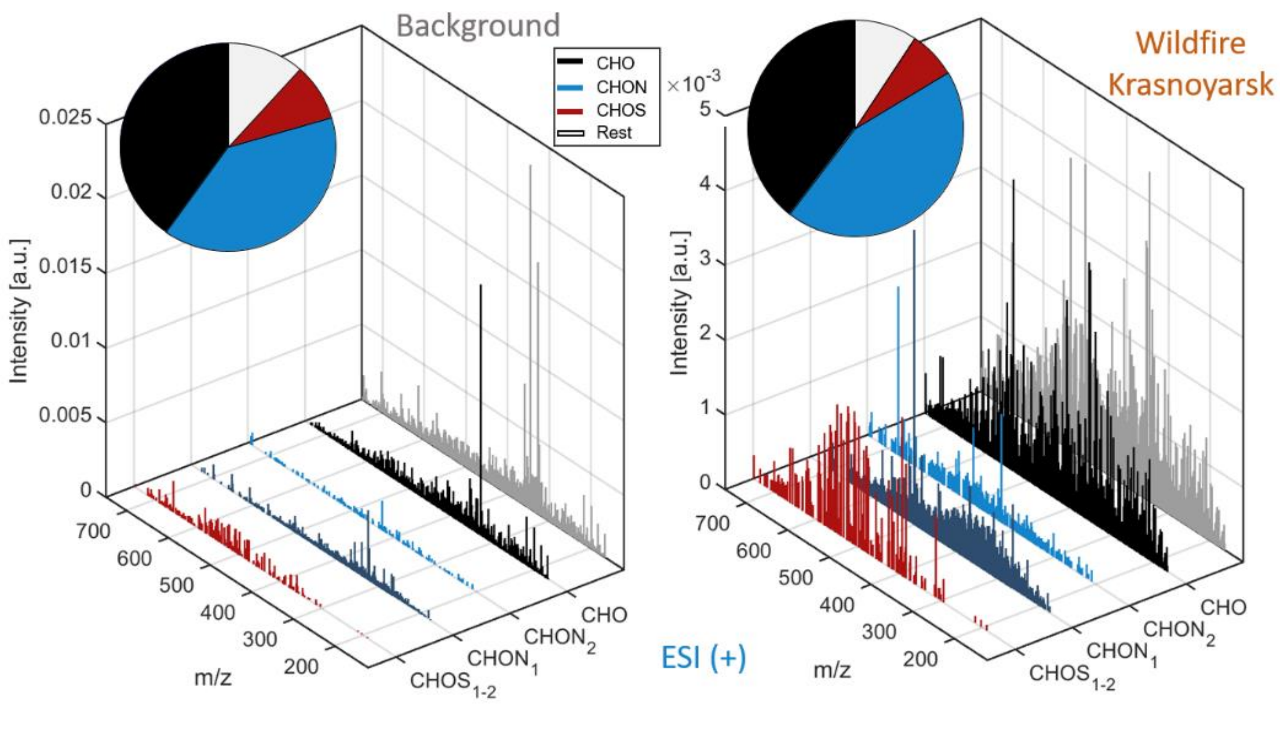

Figure S7. ESI (+)-FTICR mass spectra of exemplary *background* (left, *Sample 10*) and Krasnoyarsk region wildfire influenced (right, *Sample 20)* filter extract, normalized to TIC, as well as pie charts of the relative sum formula number of each compound class. Only CHO (black), CHON (blue) and CHOS (red) species are shown.

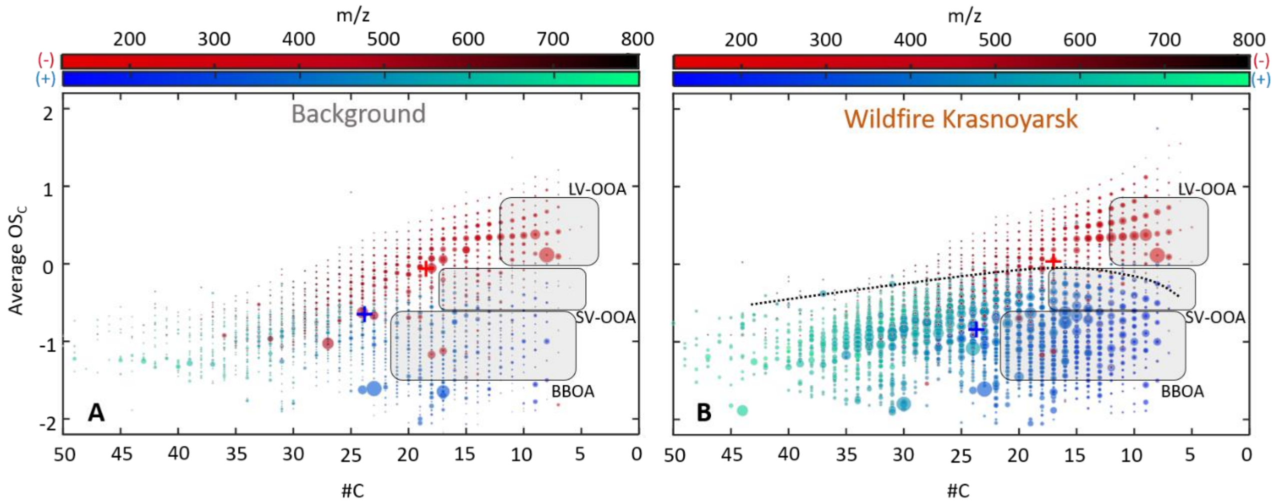

Figure S8.Average OS_C vs carbon number plot of exemplary *background* and *Krasnoyarsk-wildfire* affected ambient aerosol filter extract (*Sample 10/20*, ESI+/-: blue-green /red-black) with *potential* organic aerosol classes marked grey, the weighted average value marked with a cross (ESI+/-: blue/red) and *m/z* value indicated by the colormaps. ESI+ with high abundance of molecules in the semi-volatile oxidized organic aerosol (SV-OOA) and biomass burning organic aerosol (BBOA) classes. ESI-with highest abundance in the low-volatility oxidized organic aerosol (LV-OOA) class.

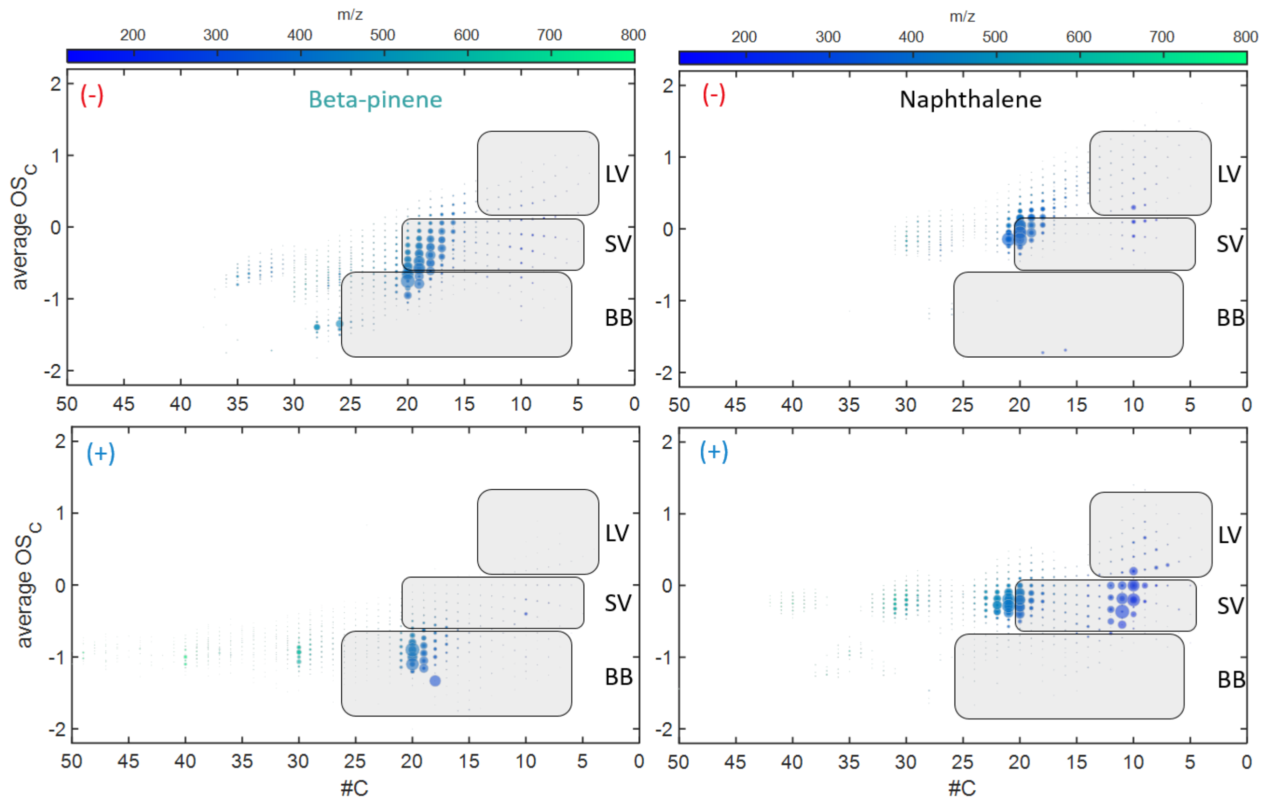

Figure S9: OS$_C$ vs carbon number plot of beta-pinene (left) and naphthalene (right) SOA from precursor ageing (ESI-/+, top/bottom) with potential organic aerosol classes marked grey and m/z value indicated by the colormap.[6]

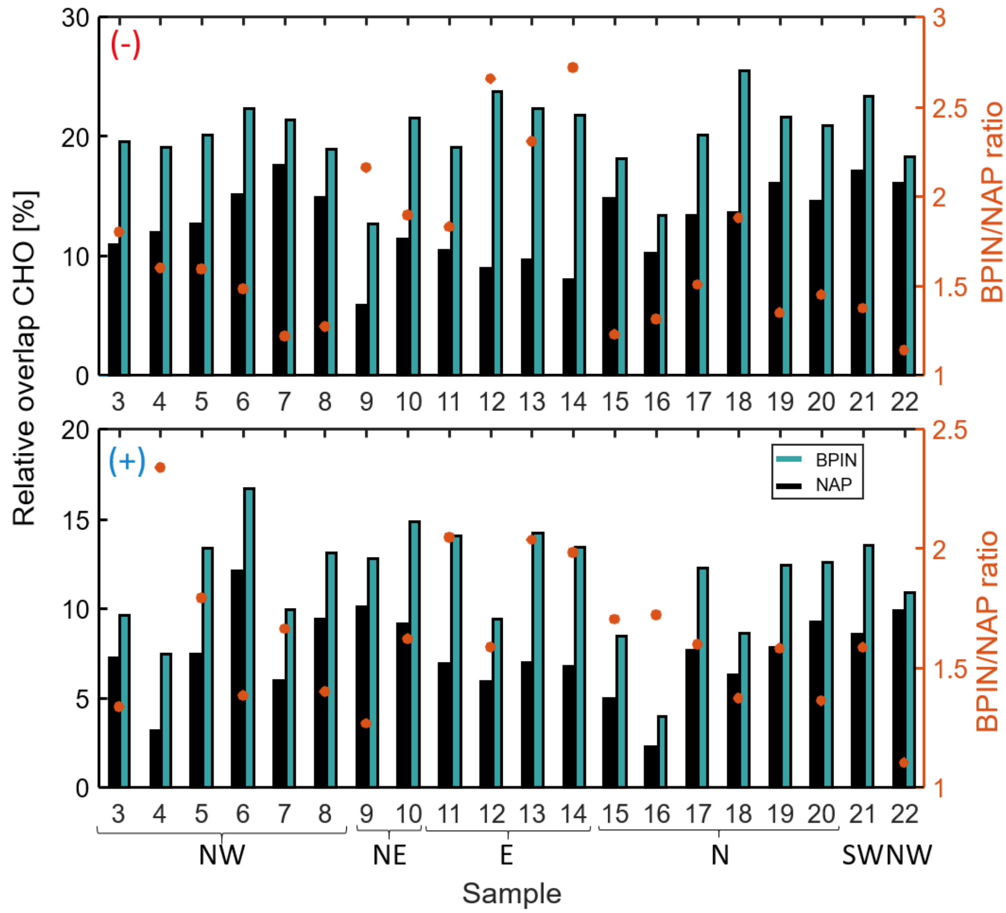

Figure S10 Bar plot of the relative overlap of CHO sum formulae of each ambient aerosol filter extract with filter extract from beta-pinene (green) and naphthalene (black) precursor ageing. Orange dots indicate the ratio of BPIN to NAP relative overlap. Samples are assigned with the wind direction during their sampling.

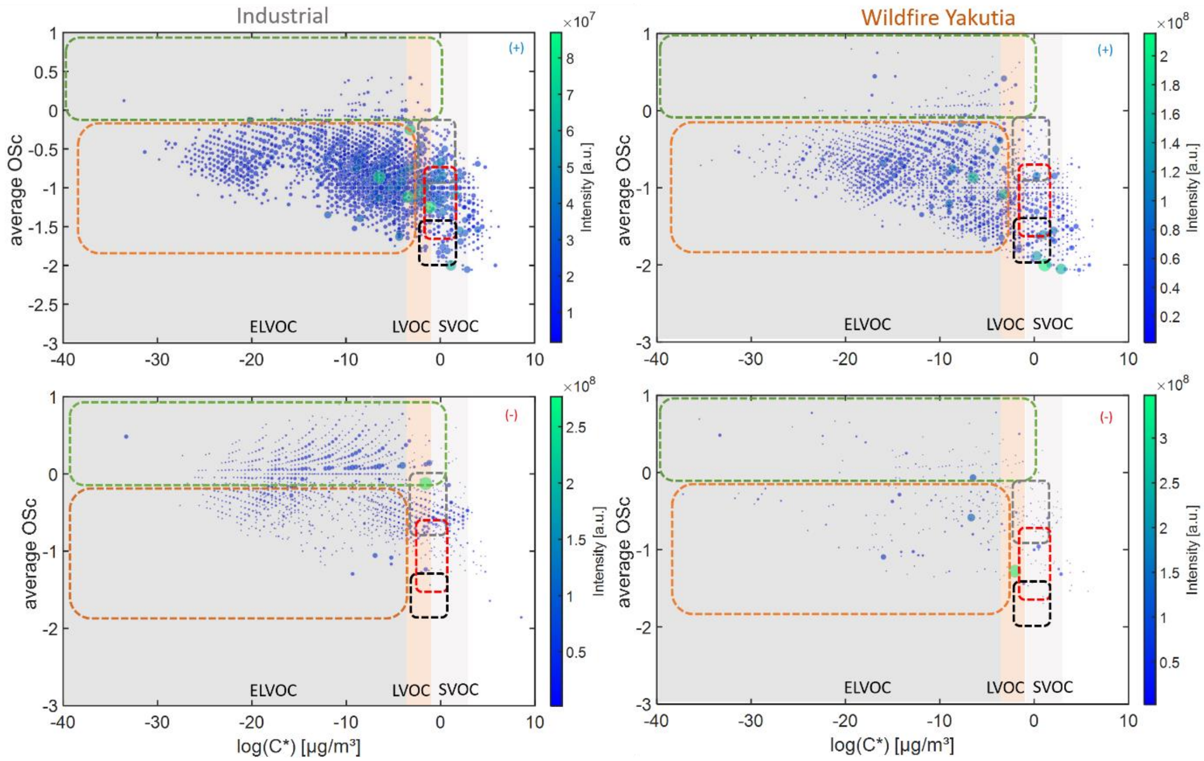

Figure S11: Calculated volatility (saturation concentration, C^* [μg/m³]) and OS_C of identified molecular formulae (ESI+ top ESI- bottom) in *Sample 6* (industrial, left) and *Sample 16* (WF Yakutia, right) with marked volatility ranges of semi volatile (SVOC), low volatility (LVOC) and extremely low volatility organic compounds (ELVOC). Coloured squares represent areas of oxidized organic aerosol (LV green, SV purple), biomass-burning organic aerosol (BBOA, red), hydrocarbon-like organic aerosol (HOA) and oligomers (orange).[4]

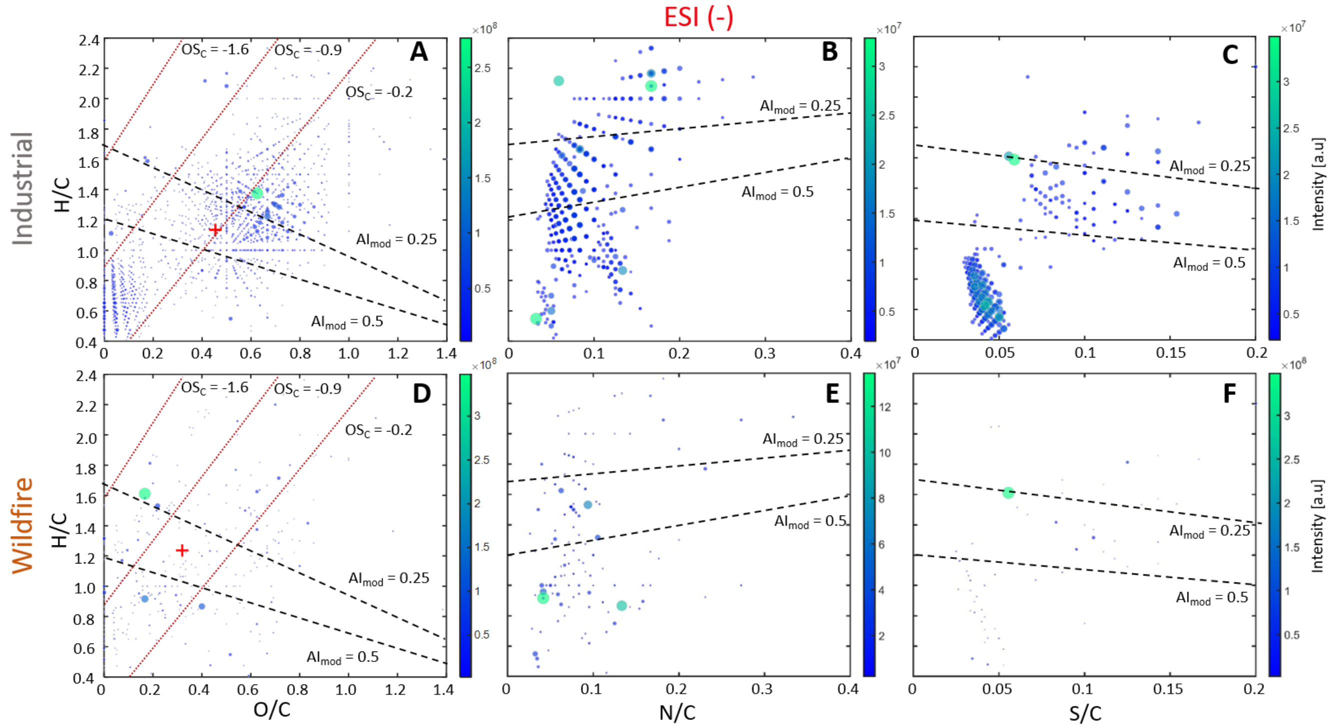

Figure S122. Van-Krevelen plots of exemplary industrial (*Sample 6, top*) and WF (*Sample 16, bottom*) samples in negative ionization mode. **A, D**: O/C vs H/C ratios of all sum formulae in ESI- with intensity weighted average O/C and H/C ratio marked red. **B**, **E**: N/C vs H/C ratios of nitrogen containing sum formulae found in urban and wildfire filter extract in ESI-. **C**, **F:** S/C vs H/C ratios of sulphur containing sum formulae.

References

(1) Popovicheva, O.; Molozhnikova, E.; Nasonov, S.; Potemkin, V.; Penner, I.; Klemasheva, M.; Marinaite, I.; Golobokova, L.; Vratolis, S.; Eleftheriadis, K.; Khodzher, T. *J. Environ. Sci.* **2021**, DOI: 10.1016/j.jes.2021.01.011.

(2) Li, Y.; Pöschl, U.; Shiraiwa, M. *Atmos. Chem. Phys.* **2016**, DOI: 10.5194/acp-16-3327-2016.

(3) Zeng, Y.; Ning, Y.; Shen, Z.; Zhang, L.; Zhang, T.; Lei, Y.; Zhang, Q.; Li, G.; Xu, H.; Ho, S. S. H.; Cao, J. *J. Geophys. Res. Atmos.* **2021**, DOI: 10.1029/2021JD034791.

(4) Kew, W.; Blackburn, J. W. T.; Clarke, D. J.; Uhrín, D. *Rapid commun. Mass Spectrom.* **2017**, DOI: 10.1002/rcm.7823.

(5) Kalberer, M.; Paulsen, D.; Sax, M.; Steinbacher, M.; Dommen, J.; Prevot, A. S. H.; Fisseha, R.; Weingartner, E.; Frankevich, V.; Zenobi, R.; Baltensperger, U. *Science* **2004**, DOI: 10.1126/science.1092185.

(6) Pardo, M.; Offer, S.; Hartner, E.; Dibucchianico, S.; Bisig, C.; Bauer, S.; Pantzke, J.; Zimmermann, E.; Cao, X.; Binder, S.; Kuhn, E.; Huber, A.; Jeong, S.; Käfer, U.; Schneider, E.; Meščeriakovas, A.; Bendl, J.; Brejcha, R.; Buchholz, A.; Gat, D.; Hohaus, T.; Rastak, N.; Karg, E.; Jakobi, G.; Kalberer, M.; Kanashova, T.; Hu, Y.; Ogris, C.; Marsico, A.; Theis, F.; Shalit, T.; Gröger, T.; Rüger, C.; Öder, S.; Orasche, J.; Paul, A.; Ziehm, T.; Zhang, Z.-H.; Adam, T.; Sippula, O.; Sklorz, M.; Schnelle-Kreis, J.; Czech, H.; Kiendler-Scharr, A.; Zimmermann, R.; Rudich, Y.*, under review*.